

Summary of NIKA2 calibration files for the PIIC data reduction software

S. Berta and R. Zylka
April 14th, 2020

Last update: December 15th, 2021

PIIC calibration files for NIKA2

In order to process NIKA2 data, PIIC needs a set of calibration files, that describe the properties of the kinetic inductance detectors (KIDs) array: geometry, resonance frequencies, cross-talking, response to incoming light (i.e. flux calibration). These are called “*data associated files*” (DAFs) and can be retrieved from the GILDAS download pages.

At each new release of PIIC, the DAFs database is included in the PIIC package.

After each observing pool, the PIIC support team processes calibration data and produces new calibration files. The DAFs database is thus updated and a new version is available online, in a separate tar-ball, independent of the PIIC package. Therefore, when browsing the PIIC GILDAS pages for updates, always check for new PIIC and DAFs tar-balls.

DAFs content

The PIIC DAFs consist of five different main types of files. In alphabetical order:

- calibration files (CAL), defining the response of KIDs for flux calibration after flat fielding;
- deleted receiver pixels (DRP) files, listing those KIDs that are known to cross-talk;
- frequency files (NKFR), listing the natural resonance frequencies of all KIDs, for different *sweeps*¹;
- receiver pixels parameters (RPP), listing the main parameters defining the KIDs for each sweep;
- atmospheric conditions over all observing runs (TAU files), i.e. the values of the zenith opacity τ , as produced by the observatory’s tau-meter and converted to the 2 mm and 1 mm NIKA2 bands.

DAFs production

The PIIC DAFs are constructed starting from calibration scans taken during the NIKA2 observing sessions. This operation is done by the PIIC support team and is completely transparent to the users.

The flux calibration files (CAL) simply contain a constant that translates the instrumental units into physical units. They are produced starting from observations of standard calibrators (primary/secondary), such as planets or other well known sources. Dedicated small-maps, as well as pointing and focus scans are used to derive and verify the flux calibration factors.

The list of DRPs is built and regularly updated via visual checks of the cross-talking KIDs, based on beam-maps. A new list is defined for each new sweep. However, as the resonance frequencies drift with aging of the KIDs, more than one list per sweep might be necessary through time. The DRPs list only the strongest cross-talks, i.e. above 5% of flux “transfer”. This is a “static” list of KIDs to be excluded. During the data processing, additional selection criteria apply and more KIDs are rejected based – for example – on tuning angle, r.m.s. along the timeline, stability, etc.; this is a “dynamic” list of discarded KIDs, that may differ for each scan.

¹ a sweep is practically a re-definition of KIDs resonance frequencies, performed regularly for each new season.

KIDs resonance frequencies (NKFR) are an intrinsic characteristic of the detectors and are defined at each new *sweep*. They are thus basically an input information, that does not need to be computed a posteriori by the PIIC team. They're used to check if the DAFs are valid for the given observing pool.

The receiver pixels parameters (RPP) files define the major parameters required for data processing: the position of each KID in the field of view of NIKA2, the forward and main beam “flat-fields”, flags, etc. Each KID is identified in resonance-frequency space, therefore its spatial position is not known a priori. Beam maps are used to derive the KIDs positions in the FoV. The order of KIDs in resonance frequency is re-shuffled at each new *sweep*, therefore new RPPs (as DRPs) are needed at least at each new sweep.

Finally, tau-meter files are provided by the observatory after each NIKA2 observing run. They are used to produce the TAU files for the 2 mm and 1 mm NIKA2 bands.

Notes about the quality of calibration

Calibration scans (beam maps, flux calibrators maps, pointing, focus) are processed after each observing run. Different runs and scans are observed under different conditions (e.g. atmospheric and instrumental), hence for some pools the calibration scans are more accurate than for others.

Several factors can contribute to the quality of DAFs (RPPs, CAL, ...):

- The fine position of KIDs in the FoV depends on focus. The focal surface is not flat, but at 1 mm has variations of up to ~ 0.7 mm from the center to the edges of the Array. Because of this, the effective beam positions may differ from the ones given in the RPPs. The discrepancy might be even $>FWHM/2$, especially in the upper-left part of the FoV.
- Gain-elevation dependence (see J. Peñalver reports² of 2012), due to homologous deformations generated by gravity. This is one component of astigmatism depending on telescope Elevation. The structural distortions are minimal for an Elevation of ~ 50 deg and operate in different perpendicular directions at lower/higher Elevations. When off-focus, the astigmatism worsens.
- Non-homologous deformations – now larger than in the past – visible as an effect of the temperature of the telescope, whose structure and surface deform under the irradiation of the sun.
- Different observing methods or strategies and different map sizes also affect the calibration: because of the changes of focus across the FoV, maps of different sizes (e.g. pointings vs. small maps on calibrators), will not give the same results for the same value of atmospheric opacity, as different KIDs “see” the source.
- Because of the above-mentioned reasons and because of sky conditions, observations taken at different times of the day have different quality (beam shape, flux calibration r.m.s., stability, etc.). Telescope distortions are exasperated during day time, and sky stability is poor. The statistics Table includes r.m.s. Values for day+night and night-only calibrator observations. In Figure 4 an example (NIKA2 run 14) is shown.
- Finally, some observing periods benefitted from better general observing conditions than others, e.g. better weather conditions and a more optimal combination of all factors listed above. Different “selection criteria for performing the observations” might have been applied in different observing pools, e.g. accepting the telescope or weather conditions, because of different team present at the telescope, or other contingency reasons.

2 http://www.iram.es/IRAMES/mainWiki/AstronomerOfDutyChecklist#Gain_elevation_correction

DAFs choice

The philosophy of the PIIC team is to use the best possible DAFs for each run. Consequently, even if calibration scans are analyzed for each run and new RPP/CAL/DRP are produced, the DAFs to be used to reduce the science data of a given pool were not necessarily taken during that same pool.

Unless a new instrumental configuration comes into play (e.g. a new sweep, optics changes, hardware modifications, etc.), if the new calibration files obtained during the given pool are not better than the previous ones, we keep using the best (older) DAFs.

This holds if no significant changes in geometry or flux calibration are detected. For this reason, in the analysis process of each new run, the current geometry, flux calibration and cross-talking are always verified against the best DAFs valid for that instrumental setup, and only if no significant changes are present the old ones can be kept.

Reality can be different

The analysis described so far, Table 2, and Figures 1, 2, 3 and 4 are based on the best scans performed on calibrators in each run. These were selected on the basis of the source profile FWHM and other factors, thus excluding defocused and poor quality scans. In reality, as mentioned before, science observations are not always taken under ideal observing conditions.

To give an idea of the possible effects on calibration, in Figure 5 we show two recent examples for which they are well visible: the NIKA2 runs 47 and 51. In this case, all the scans performed on calibrator are plotted, including pointing scans and focus sequences (i.e. also the de-focused scans). Starting with run 45, these effects became more severe.

Since the beam during the day is often distorted, in Fig. 5, the integrated flux (i.e. an aperture flux) is shown, instead of the main beam flux. The Figure shows the integrated flux as a function of: scan running number, highlighting day (red) and night (blue) scans; UT; extinction correction; average size of the source profile.

During the day the telescope distorts and the beam is broadened and suffers for stronger astigmatism. Consequently, the flux loss at a fixed aperture becomes large and only a fraction of the total flux of the calibrators is measured. The diagonal trends (in a saw-teeth shape) on the upper panels of Fig. 5 exemplify this effect.

Note that focus sequences appear here as small groups of 5 data points closely aligned diagonally. The spread in the retrieved flux fraction of a focus sequence is smaller than the general calibration spread over the whole diagram, therefore it is still possible to use focus scans here.

The panels in the second row of Fig. 5 confirm that – during runs 47 and 51 – only a limited number of scans was taken on calibrators during nights.

In the third row of panels, the apparent trend of the recovered flux fraction to decrease as a function of extinction correction in run 47 is misleading. This trend does not reflect a real dependence of calibration on extinction correction, but it rather hides the dependence on day/night conditions. In fact, also here day/night times are marked with red/blue dots. The strongest flux losses are again systematically during the day. In the data of run 51 this apparent trend with extinction correction is less evident because the scatter in the recovered flux is much larger, despite the very low values of $\tau < 0.15$ at the zenith. It seems that the telescope suffered from severe distortions not only during the day (the weather was excellent, and the sun illumination was thus stronger), but also during the night (for reasons still to be investigated).

The bottom panels in Fig. 5 show how the flux loss depends on the FWHM of the source profile, with no need for an exhaustive explanation.

The calibration scans (i.e. *calib1scan*) are marked with stars in Fig. 5.

Finally Fig. 6 shows the main-beam calibration of all scans taken on calibrators (including pointing and focus), limited to in-focus scans only, for all observations taken in NIKA2 runs 34 to 51. Significant drifts spanning up to 2-3 weeks can be seen. The cause of these drifts is to date still unknown.

Availability table

Here we summarize, for each NIKA2 science pool, and only for science pools, some basic information about the NIKA2 instrumental setup and the content of PIIC DAFs. For the latter, the number of used beam maps and flux calibrator scans are specified, as well as whether DAFs are available and in which run the adopted RPP/CAL files were built.

Table 1: basic information about NIKA2 science pools and the related DAFs

[illegible]

Run* Nika2/Cryo	Dates	DAQ version	Sweep	# Beam maps	# Flux Calib.**	Calib.*** processed	DAFs available	RPP version	Flux calib version
36/49	2019/10/29 2019/11/04	1	Ar2 2019/09 Ar1&3 2019/03	9	Ar2 50 Ar1 22 Ar3 25	y	y	Ar2 Run 34 Ar1 Run 34 Ar3 Run 34	Ar2 Run 12 Ar1 Run 23 Ar3 Run 34
37/49b	2019/11/05 2019/11/12	1	Ar2 2019/09 Ar1&3 2019/03						
38/50	2019/12/10 2019/12/17	1	Ar2 2019/09 Ar1&3 2019/03	3	Ar2 50 Ar1 41 Ar3 32	y	y	Ar2 Run 34 Ar1 Run 34 Ar3 Run 34	Ar2 Run 38 Ar1 Run 38 Ar3 Run 38
39/51	2020/01/14 2020/01/21	1	Ar2 2019/09 Ar1&3 2020/01	4	Ar2 45 Ar1 43 Ar3 42	y	y	Ar2 Run 34 Ar1 Run 39 Ar3 Run 39	Ar2 Run 38 Ar1 Run 38 Ar3 Run 38
40/52	2020/01/28 2020/02/04	1	Ar2 2019/09 Ar1&3 2020/01	9	Ar2 59 Ar1 55 Ar3 50	y	y	Ar2 Run 34 Ar1 Run 39 Ar3 Run 39	Ar2 Run 38 Ar1 Run 38 Ar3 Run 38
41/53	2020/02/11 2020/02/18	3	Ar2 2019/09 Ar1&3 2020/01	7	Ar2 117 Ar1 106 Ar3 106	y	y	Ar2 Run 34 Ar1 Run 39 Ar3 Run 39	Ar2 Run 38 Ar1 Run 38 Ar3 Run 38
43/55	2020/03/10 2020/03/17	3	Ar2 2019/09 Ar1&3 2020/01	5	Ar2 41 Ar1 43 Ar3 35	y	y	Ar2 Run 34 Ar1 Run 39 Ar3 Run 39	Ar2 Run 43 Ar1 Run 43 Ar3 Run 43
45/57	2020/10/20 2020/11/03	3	Ar2 2020/10 Ar1&3 2020/10	10	Ar2 88 Ar1 74 Ar3 73	y	y	Ar2 Run 45+47 Ar1 Run 45+47 Ar3 Run 45+47	Ar2 Run 43 Ar1 Run 43 Ar3 Run 43
47/59	2020/11/17 2020/11/24	3	Ar2 2020/10 Ar1&3 2020/10	4	Ar2 79 Ar1 56 Ar3 58	y	y	Ar2 Run 45+47 Ar1 Run 45+47 Ar3 Run 45+47	Ar2 Run 43 Ar1 Run 43 Ar3 Run 43
48/60	2020/12/08 2020/12/15	3	Ar2 2020/10 Ar1&3 2020/10	3	Ar2 24 Ar1 7 Ar3 9	y	y	Ar2 Run 45+47 Ar1 Run 45+47 Ar3 Run 45+47	Ar2 Run 43 Ar1 Run 43 Ar3 Run 43
49/61	2021/01/12 2021/01/26	3	Ar2 2020/10 Ar1&3 2020/10	5	Ar2 114 Ar1 98 Ar3 92	y	y	Ar2 Run 45+47 Ar1 Run 45+47 Ar3 Run 45+47	Ar2 Run 43 Ar1 Run 43 Ar3 Run 43
50/62	2021/02/09 2021/02/23	3	Ar2 2020/10 Ar1&3 2020/10	11	Ar2 75 Ar1 62 Ar3 61	y	y	Ar2 Run 45+47 Ar1 Run 45+47 Ar3 Run 45+47	Ar2 Run 43 Ar1 Run 43 Ar3 Run 43
51/63	2021/03/09 2021/03/23	3	Ar2 2020/10 Ar1&3 2020/10	12	Ar2 37 Ar1 33 Ar3 32	y	y	Ar2 Run 45+47 Ar1 Run 45+47 Ar3 Run 45+47	Ar2 Run 43 Ar1 Run 43 Ar3 Run 43
52/64	2021/05/28 2021/05/29	3	Ar2 2020/10 Ar1&3 2020/10	0	n/a	n	y	Ar2 Run 45+47 Ar1 Run 45+47 Ar3 Run 45+47	Ar2 Run 43 Ar1 Run 43 Ar3 Run 43
55/67	2021/10/26 2021/11/09	3	Ar2 2021/10 Ar1&3 2021/10	16	Ar2 176 Ar1 141 Ar3 151	y	y	Ar2 Run 55+56 Ar1 Run 55+56 Ar3 Run 55+56	Ar2 Run 43 Ar1 Run 43 Ar3 Run 43
56/68	2021/11/15 2021/11/30	3	Ar2 2021/10 Ar1&3 2021/10	6		y	y	Ar2 Run 55+56 Ar1 Run 55+56 Ar3 Run 55+56	Ar2 Run 43 Ar1 Run 43 Ar3 Run 43

* only science pools are listed

** calib. and pointing scans that made it to the shown plots

*** beam maps *and* flux calibrators

Statistics table

Here we summarize few additional pieces of information about the calibration files, namely the r.m.s. of the flux calibration and the number of identified DRPs. Figures are shown at the end of this document.

As described in the previous Sections, the flux calibration factors are computed using the data of NIKA2 runs with the best observing conditions for a given instrumental configuration. For each other run in the same configuration, we apply the best calibration factors and we compute the statistics of the derived fluxes, as compared to the intrinsic fluxes of the calibrators (which are well known sources). The following Table lists the percentual r.m.s. around the average flux in each run. Two values are given for each case: one computed on all scans (day+night); and one computed on night-only scans. Note that no gain-elevation correction was applied while deriving these values, therefore these values shall be considered as upper limits to the real r.m.s.

DRPs are mainly cross-talking KIDs and their list is checked and updated at least at each new *sweep*.

Table 2: additional statistics of calibration files

Run* Nika2/Cryo	Dates	# Flux Calib.**	Ar2 % r.m.s. flux calib.***	Ar1 % r.m.s. flux calib.***	Ar3 % r.m.s. flux calib.***	# DRPs
12/25	2017/10/24 2017/10/31	Ar2 158 Ar1 169 Ar3 152	5.8 5.4	9.9 8.5	9.8 7.6	Ar2 105 Ar1 132 Ar3 235
14/27	2018/01/16 2018/01/23	Ar2 142 Ar1 140 Ar3 124	7.0 5.9	14.8 10.6	13.6 9.3	Ar2 105 Ar1 81 Ar3 235
15/28	2018/02/13 2018/02/20	Ar2 115 Ar1 109 Ar3 115	9.7 10.1	15.5 16.6	13.9 14.6	Ar2 105 Ar1 81 Ar3 235
17/30	2018/03/13 2018/03/20	Lost because of bad weather				
18/31	2018/05/22 2018/05/29	Ar2 26 Ar1 25 Ar3 29	2.5 2.5	3.9 3.9	3.2 3.2	Ar2 105 Ar1 81 Ar3 235
22/36	2018/10/02 2018/10/09	Lost because of DAQ v2 malfunctioning				
23/37	2018/10/30 2018/11/06	Ar2 56 Ar1 37 Ar3 41	5.2 3.9	7.8 6.1	5.9 5.1	Ar2 102 Ar1 89 Ar3 235
24/38	2018/11/20 2018/11/27	Ar2 38 Ar1 24 Ar3 21	4.8 3.3	14.5 17.1	13.1 16.3	Ar2 102 Ar1 89 Ar3 235
26/40	2019/01/15 2019/01/22	Ar2 41 Ar1 44 Ar3 44	3.4 1.0	7.1 1.4	6.0 2.3	Ar2 102 Ar1 89 Ar3 235
27/41	2019/01/29 2019/02/05	Ar2 24 Ar1 24 Ar3 22	10.2 1.3	9.2 2.8	9.4 2.8	Ar2 102 Ar1 89 Ar3 235
28/42	2019/02/12 2019/02/19	Ar2 50 Ar1 45 Ar3 46	4.8 3.3	8.8 6.3	8.2 5.9	Ar2 102 Ar1 89 Ar3 235
29/43	2019/03/05 2019/03/12	Ar2 38 Ar1 48 Ar3 43	5.2 5.5	11.4 12.4	10.1 11.9	Ar2 102 Ar1 89 Ar3 235

Run* Nika2/Cryo	Dates	# Flux Calib.**	Ar2 % r.m.s. flux calib.***	Ar1 % r.m.s. flux calib.***	Ar3 % r.m.s. flux calib.***	# DRPs
30/44	2019/03/19 2019/03/26	Ar2 36 Ar1 29 Ar3 25	3.3 3.5	8.7 4.8	7.8 6.5	Ar2 102 Ar1 89/82 Ar3 235/143
34/48	2019/10/08 2019/10/14	Ar2 128 Ar1 94	6.6	12.8	13.6	Ar2 94 Ar1 136
35/48b	2019/10/15 2019/10/22	Ar3 97	6.2	11.4	11.6	Ar3 242
36/49	2019/10/29 2019/11/04	Ar2 50 Ar1 22	9.1	19.7	17.8	Ar2 94 Ar1 136
37/49b	2019/11/05 2019/11/12	Ar3 25	9.2	20.9	18.7	Ar3 242
38/50	2019/12/10 2019/12/17	Ar2 50 Ar1 41 Ar3 32	2.3 2.3	6.5 6.0	4.2 3.7	Ar2 94 Ar1 136 Ar3 242
39/51	2020/01/14 2020/01/21	Ar2 45 Ar1 43 Ar3 42	2.8 1.7	6.3 3.3	6.4 2.2	Ar2 94 Ar1 125 Ar3 260
40/52	2020/01/28 2020/02/04	Ar2 59 Ar1 55 Ar3 50	4.6 4.8	7.0 1.9	6.5 2.5	Ar2 94 Ar1 125 Ar3 260
41/53	2020/02/11 2020/02/18	Ar2 117 Ar1 106 Ar3 106	3.6 0.5	8.8 0.1	8.3 0.5	Ar2 94 Ar1 125 Ar3 260
43/55	2020/03/10 2020/03/17	Ar2 41 Ar1 43 Ar3 35	5.3 3.9	16.3 12.7	15.1 5.6	Ar2 94 Ar1 125 Ar3 260
45/57	2020/10/20 2020/11/03	Ar2 88 Ar1 74 Ar3 73	3.7 3.8	7.8 7.1	7.2 6.7	Ar2 121 Ar1 177 Ar3 299
47/59	2020/11/17 2020/11/24	Ar2 79 Ar1 56 Ar3 58	3.0 3.2	6.6 6.3	5.8 6.2	Ar2 121 Ar1 177 Ar3 299
48/60	2020/12/08 2020/12/15	Ar2 24 Ar1 7 Ar3 9	11.1 n/a	8.4 n/a	17.1 n/a	Ar2 121 Ar1 177 Ar3 299
49/61	2021/01/12 2021/01/26	Ar2 114 Ar1 98 Ar3 92	3.7 2.6	7.8 6.5	7.7 6.6	Ar2 121 Ar1 177 Ar3 299
50/62	2021/02/09 2021/02/23	Ar2 75 Ar1 62 Ar3 61	5.0 n/a	5.9 n/a	6.5 n/a	Ar2 121 Ar1 177 Ar3 299
51/63	2021/03/09 2021/03/23	Ar2 37 Ar1 33 Ar3 32	7.1 4.6	9.6 8.2	8.9 7.4	Ar2 121 Ar1 177 Ar3 299
52/64	2021/05/28 2021/05/29	n/a	n/a	n/a	n/a	Ar2 121 Ar1 177 Ar3 299
55/67	2021/10/26 2021/11/09	Ar2 176 Ar1 141	6.2	9.2	10.2	TBD
56/68	2021/11/15 2021/11/30	Ar3 151	6.1	8.8	9.9	

* only science pools are listed

** calib. and pointing scans that made it to the shown plots

*** based on main beam flux analysis; two values of r.m.s. are given for each entry: the first is computed on all scans (day+night); the second is computed on night-only scans.

Figures of NIKA2 PIIC flux calibration statistics

see the *Summary of NIKA2 calibration files* for more details

S. Berta and R. Zylka

December 16, 2021

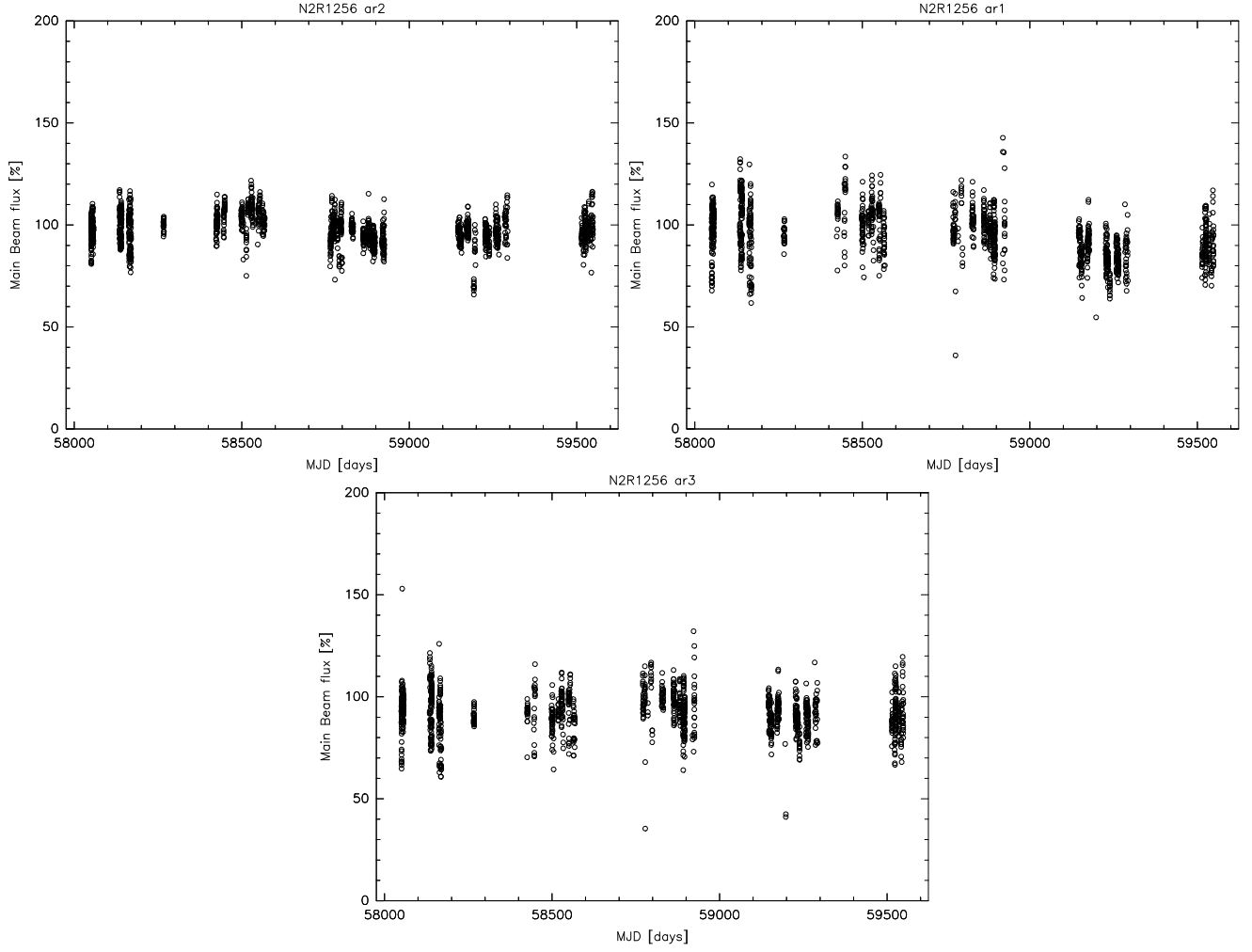


Figure 1: Distribution of the flux percentage retrieved for calibrators fitting the main beam with a Gaussian profile (black circles), for all NIKA2 science pools so far (runs 12 to 51). The three panels belong to the three NIKA2 arrays.

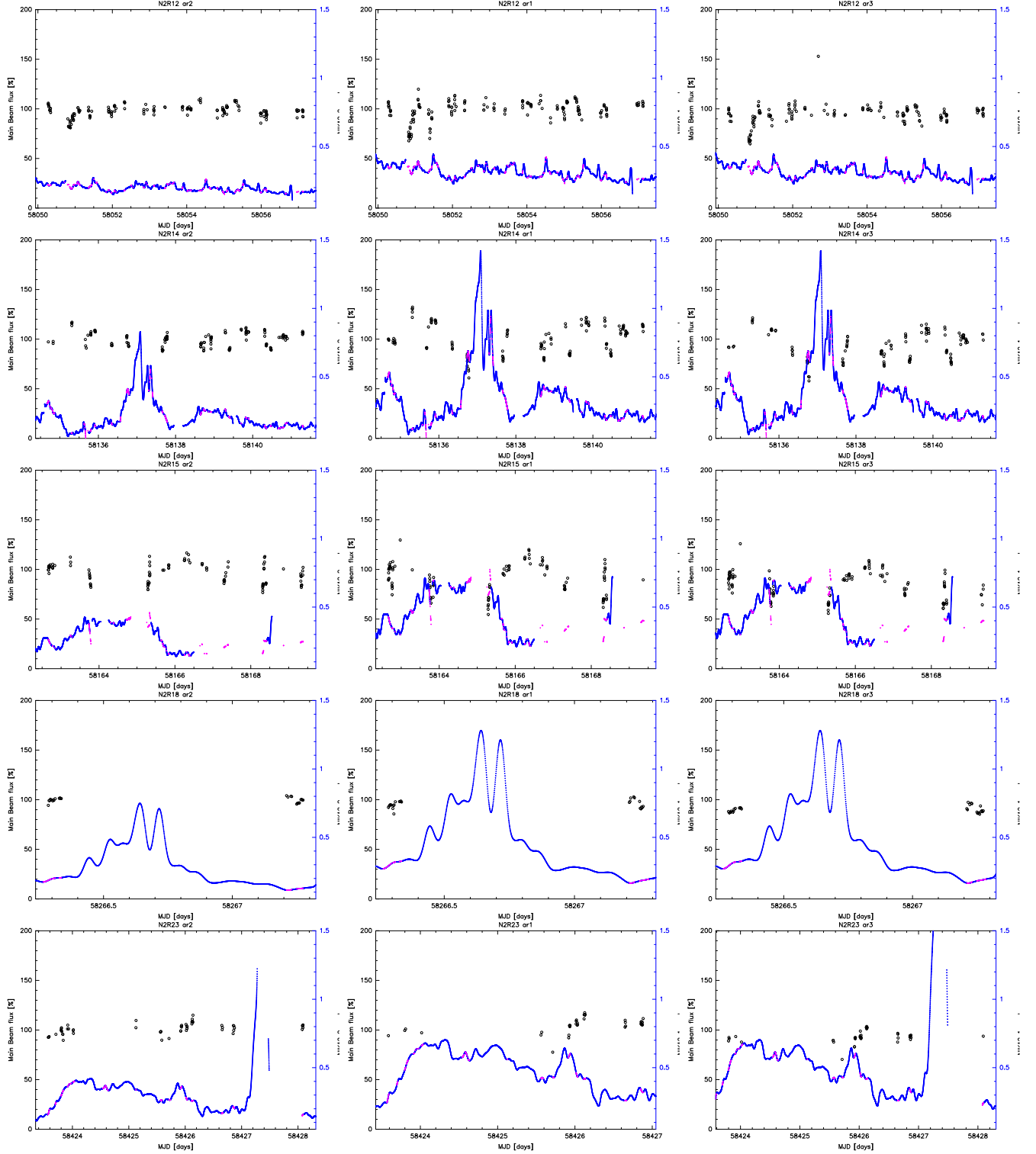


Figure 2: Same as Fig. 1, but for individual science pools: runs 12, 14, 15, 18, 23. Left, central, right panels belong to Ar2, 1, 3, respectively. The atmospheric opacity given by the tau-meter and rescaled to NIKA2 bands is shown (blue dots); in pink the opacity during a given scan is highlighted; if the tau-meter curve does not cover a scan, the value in the FITS header is used.

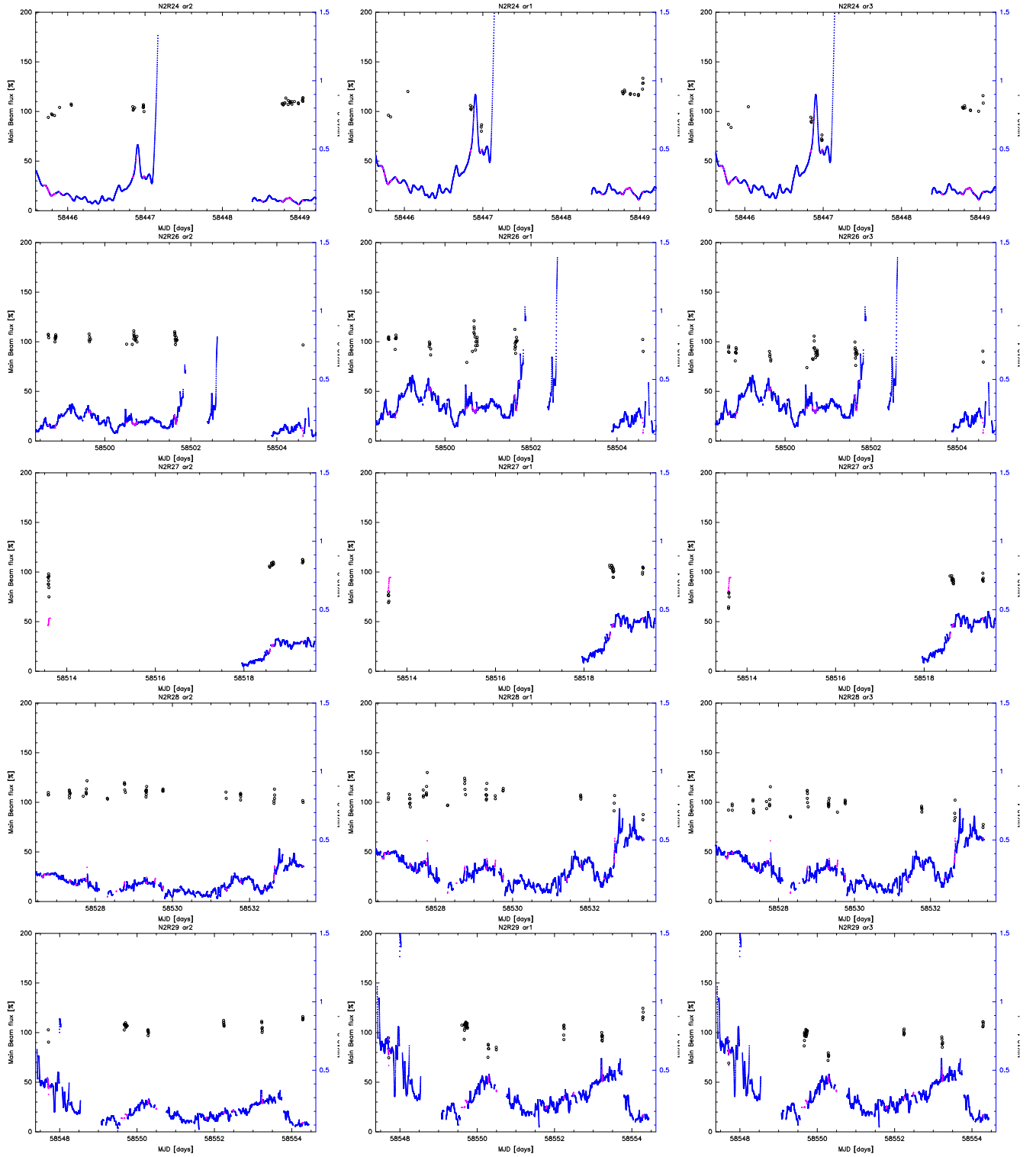


Figure 2: continued for runs 24, 26, 27, 28, 29.

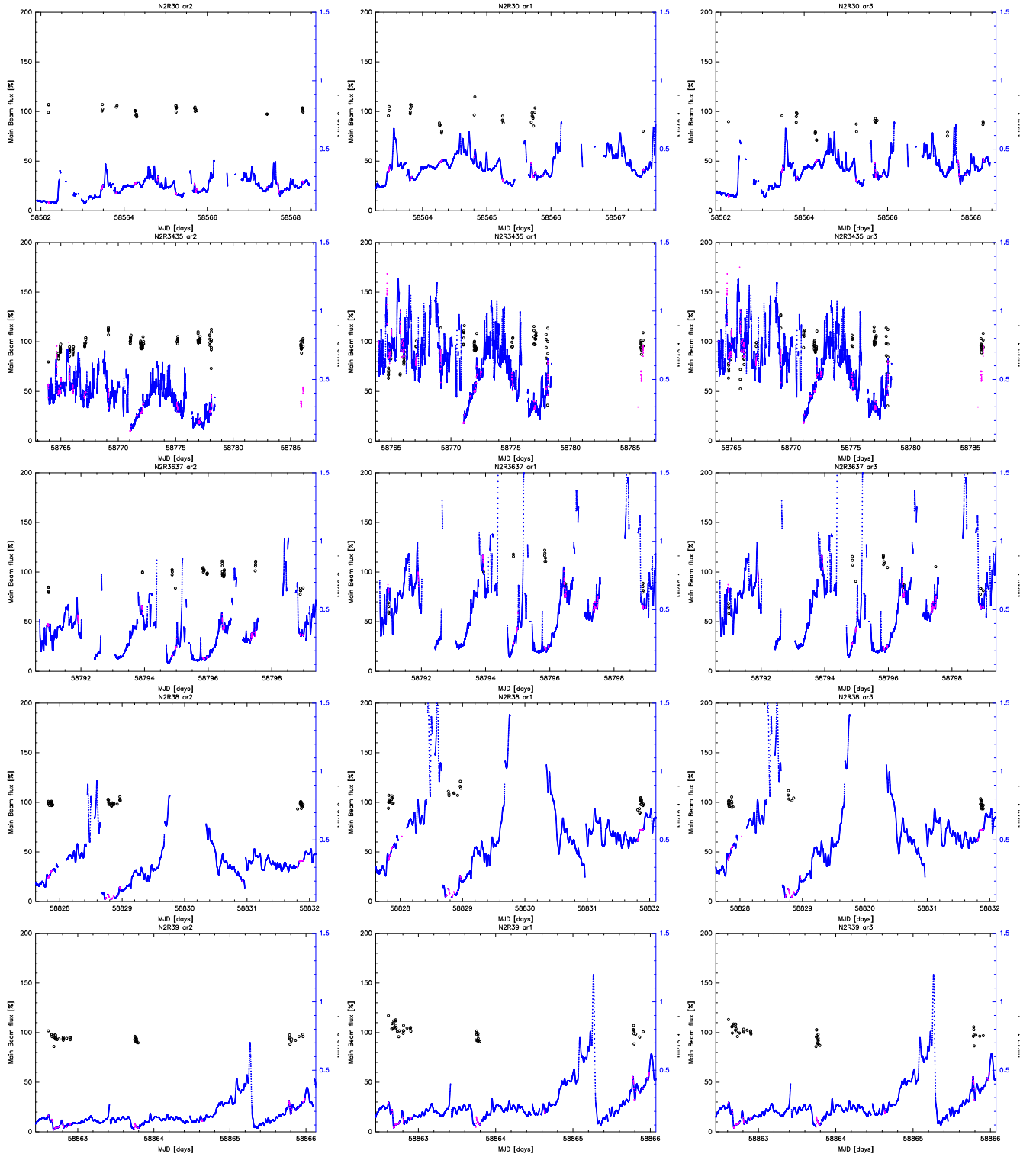


Figure 2: continued for runs 30, 34+35, 36+37, 38, 39.

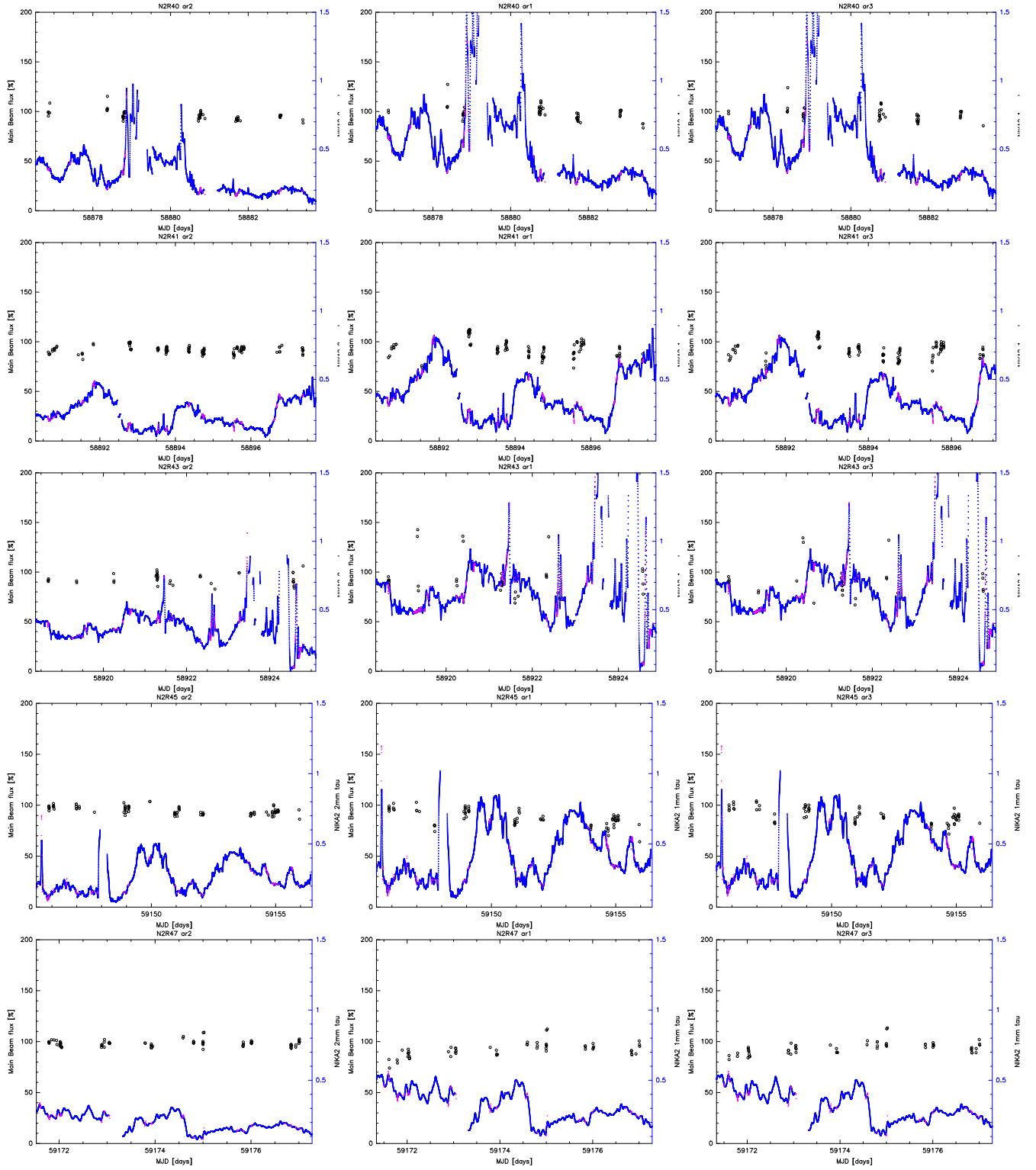


Figure 2: continued for runs 40, 41, 43, 45, 47.

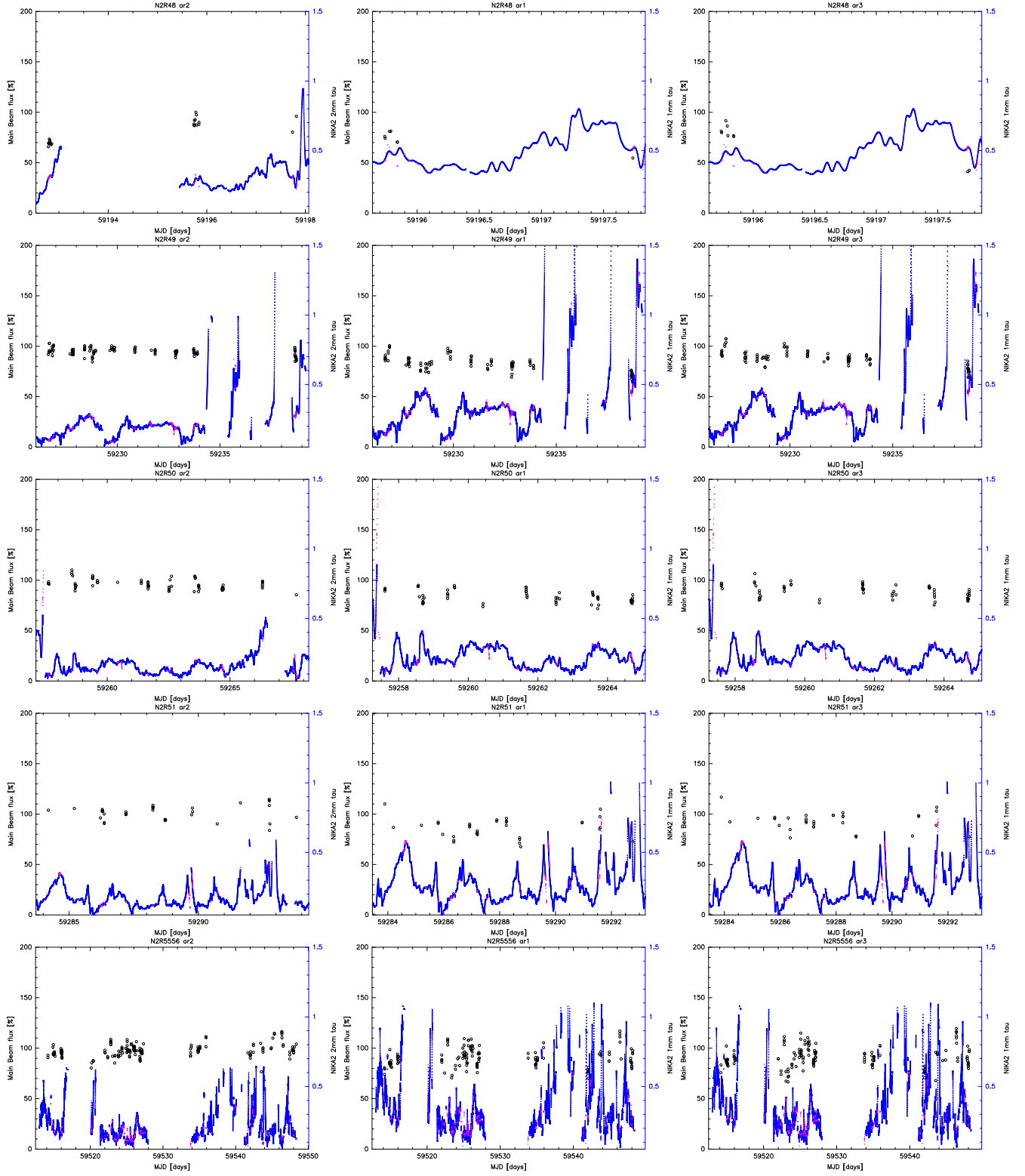


Figure 2: Continued for runs 49, 49, 50, 51, 55+56.

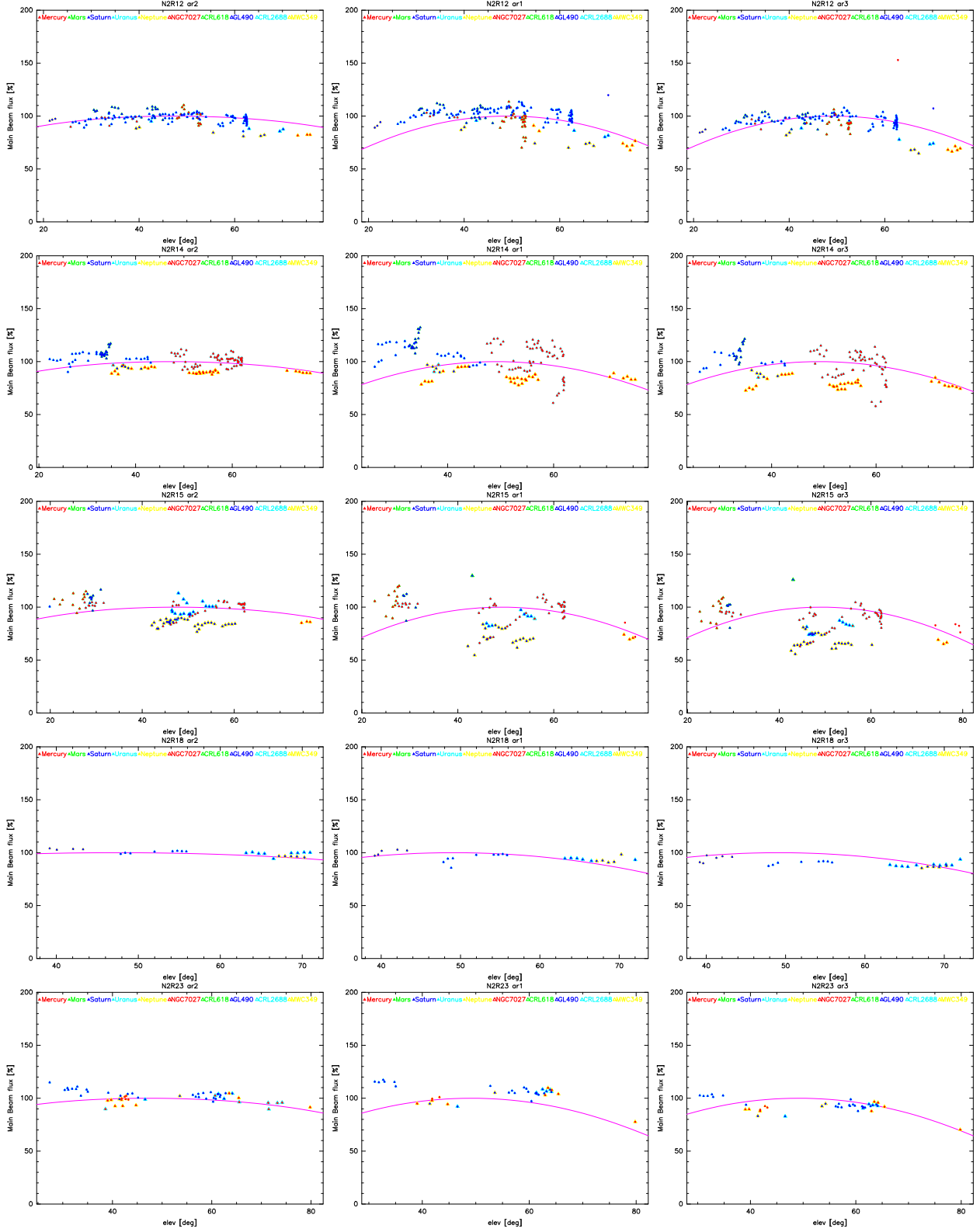


Figure 3: Main beam flux percentage (of intrinsic flux) as a function of elevation. NIK A2 runs 12, 14, 15, 18, 23. Different calibrators are depicted with different symbols/colors. Red and blue circles mark scan taken during day- and night-time, respectively. The magenta curve is the gain-elevation dependence (see J. Peñalver 2012 report).

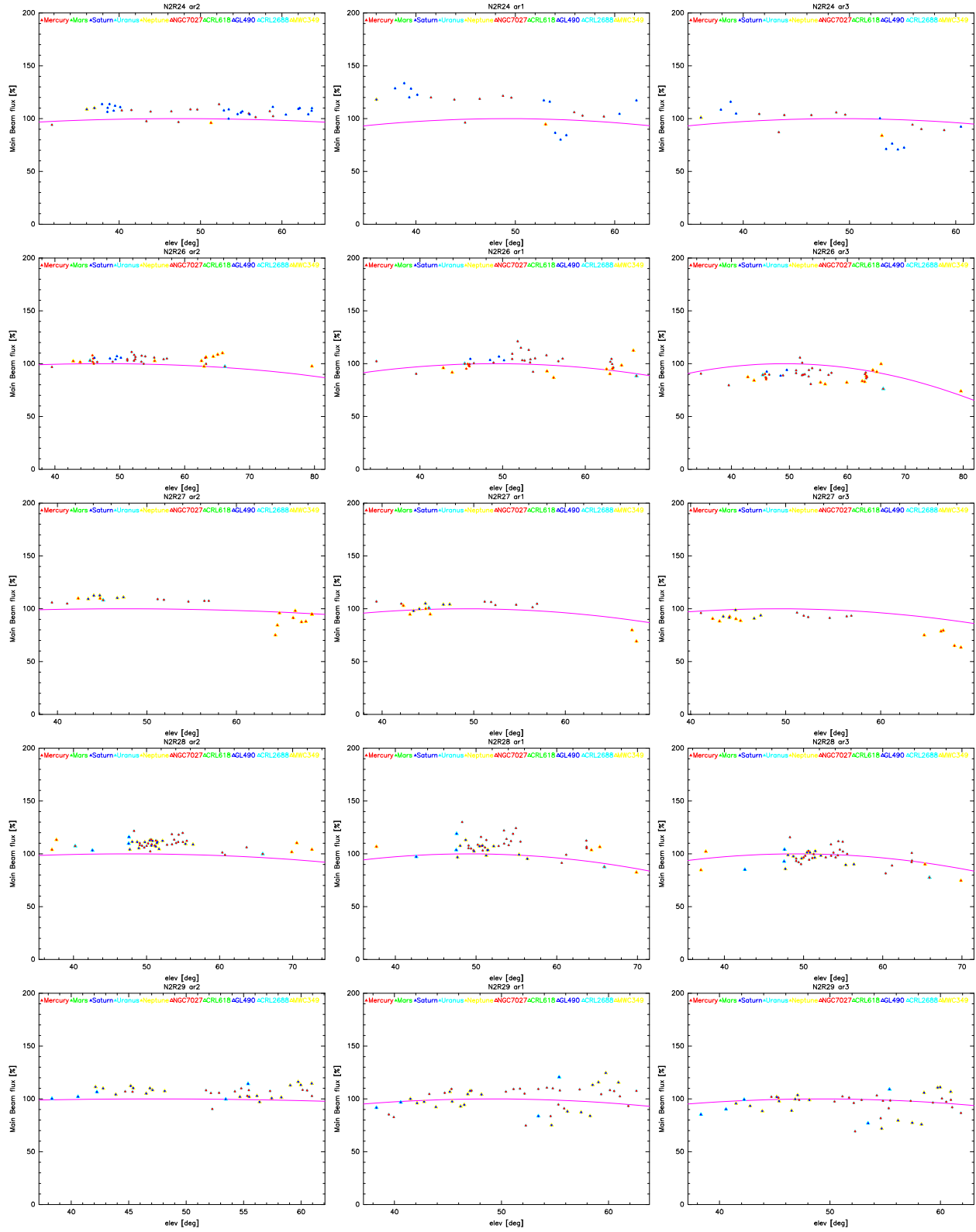


Figure 3: continued for runs 24, 26, 27, 28, 29.

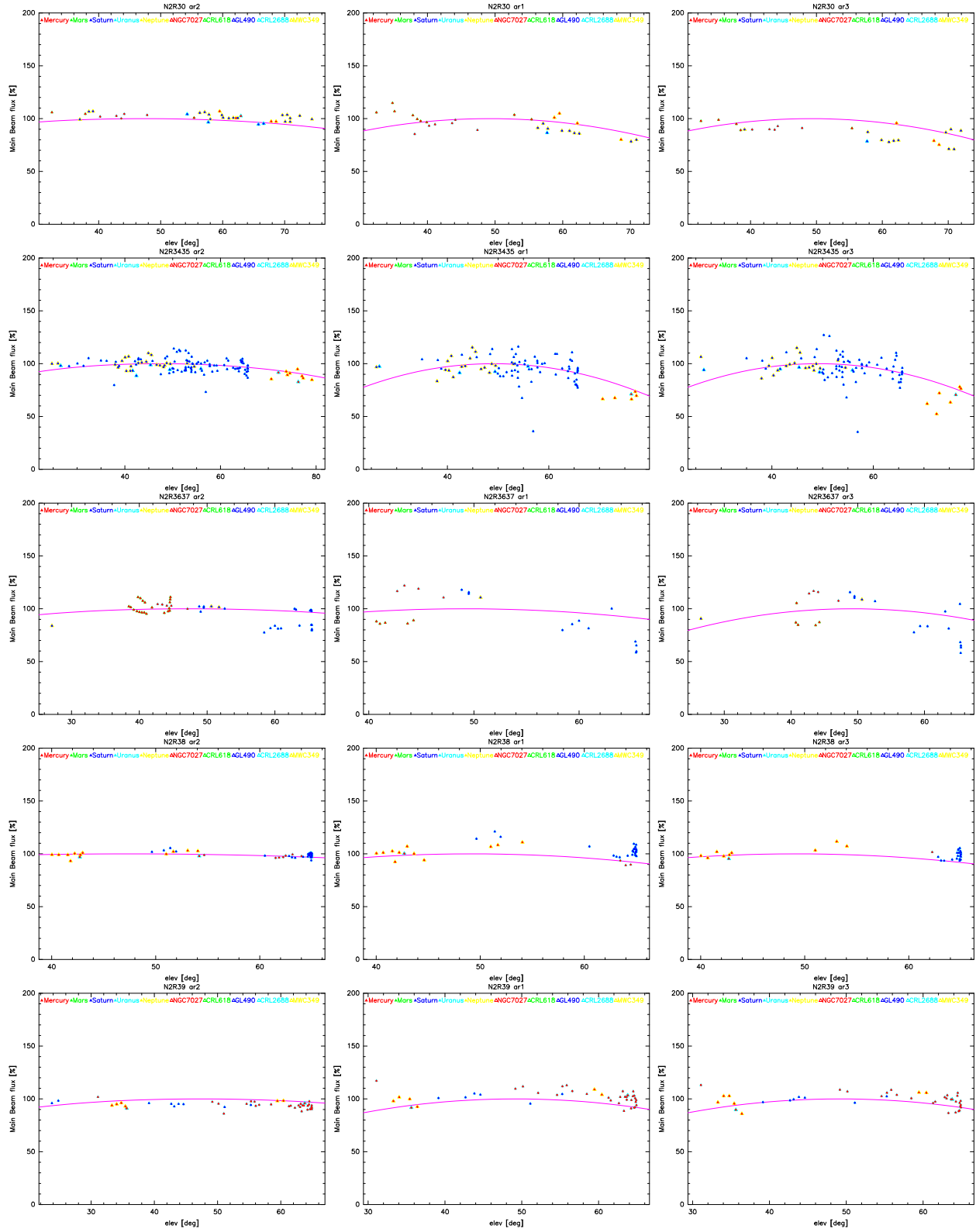


Figure 3: continued for runs 30, 34+35, 36+37, 38, 39.

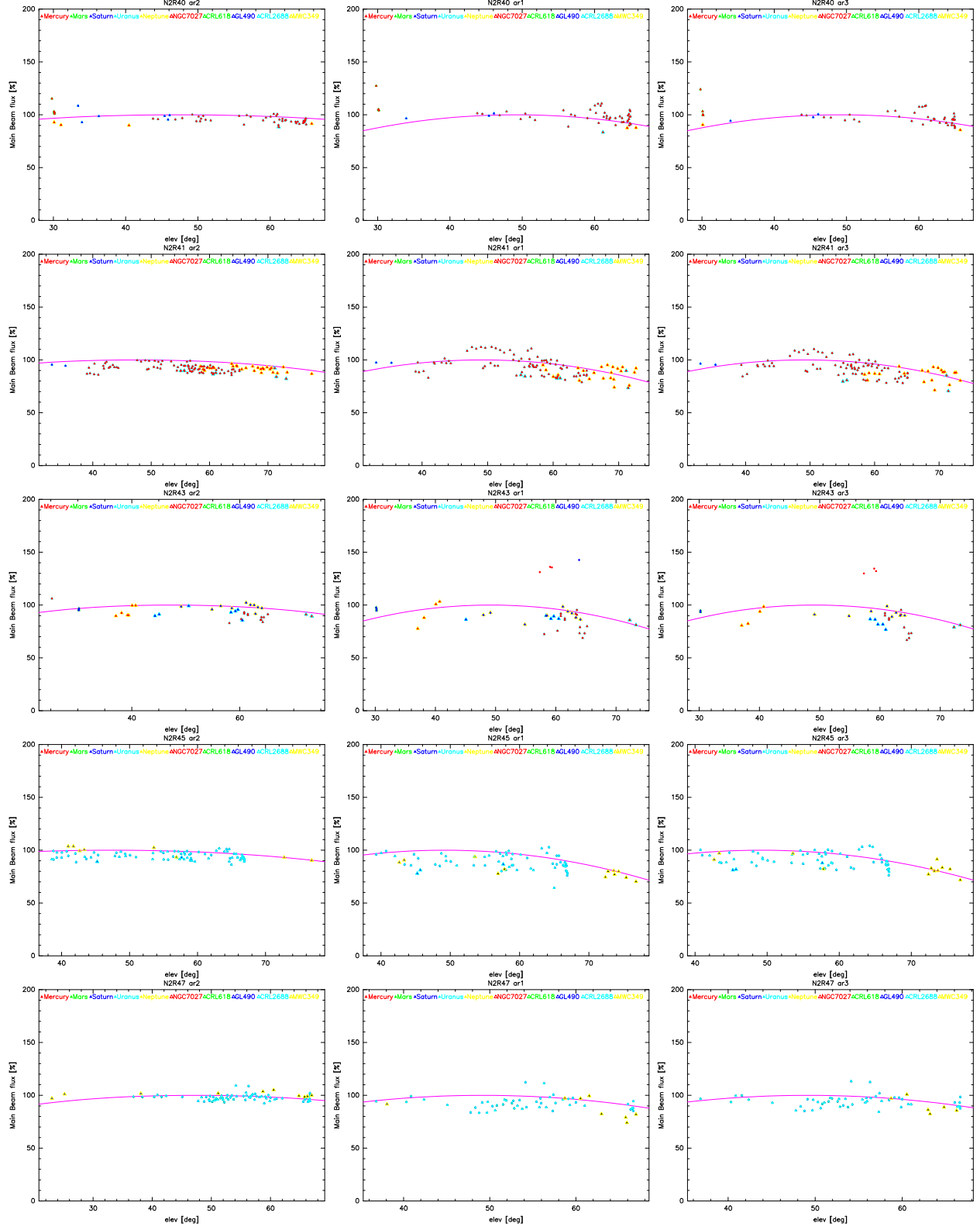


Figure 3: continued for runs 40, 41, 43, 45, 47.

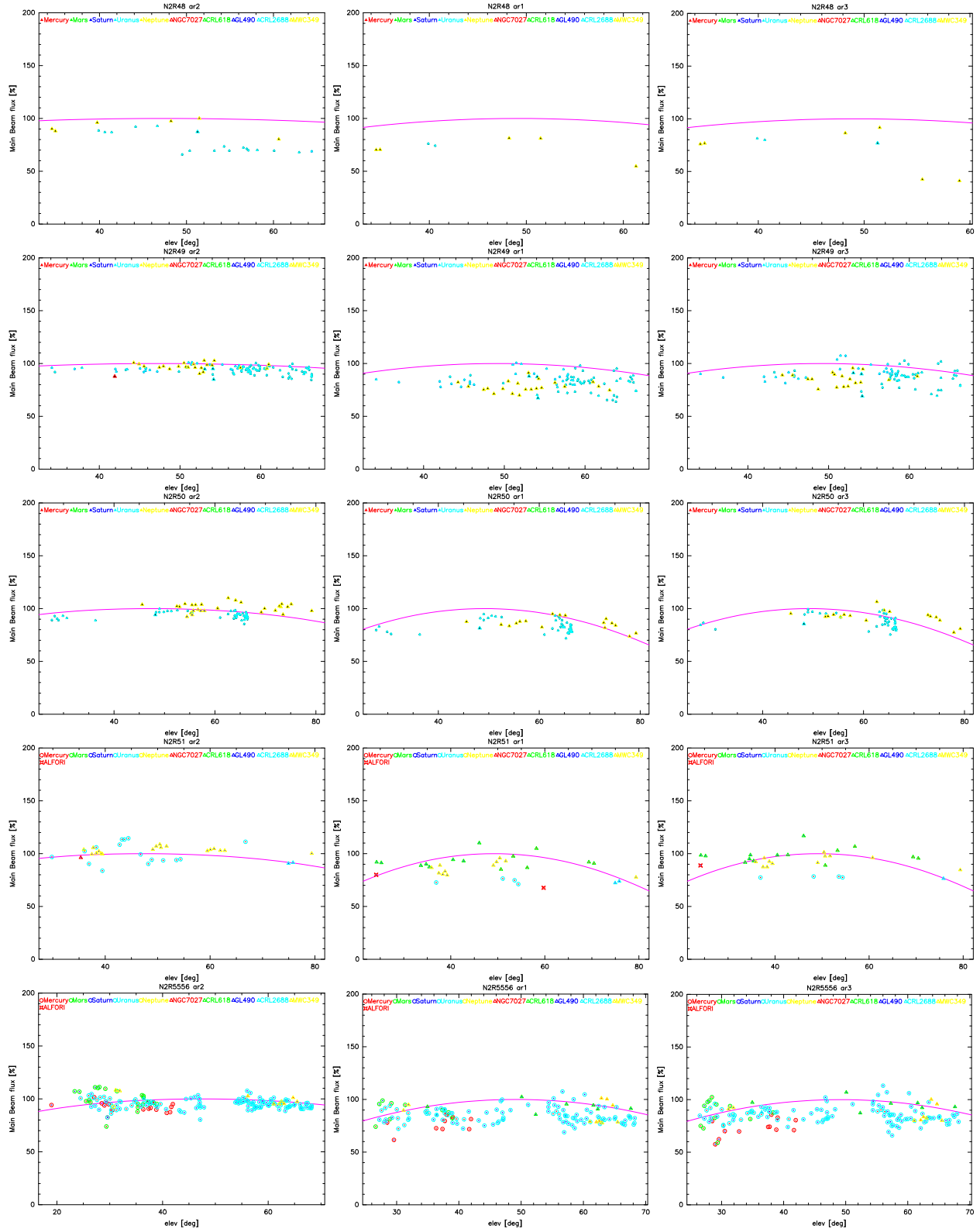


Figure 3: continued for runs 48, 49, 50, 51, 55+56.

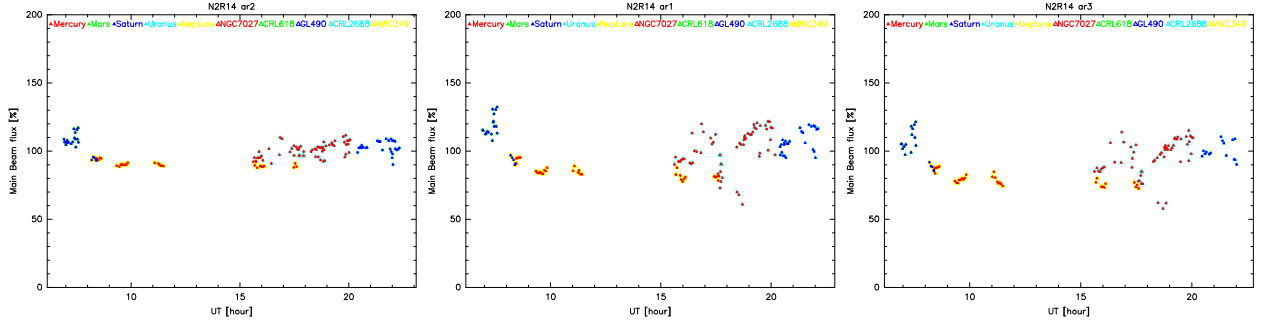


Figure 4: Main beam flux percentage (of intrinsic flux) as a function of UT, for NIK A2 run 14. Different calibrators are depicted with different symbols/colors. Red and blue circles mark scan taken during day- and night-time, respectively. A clear change between day and night is visible.

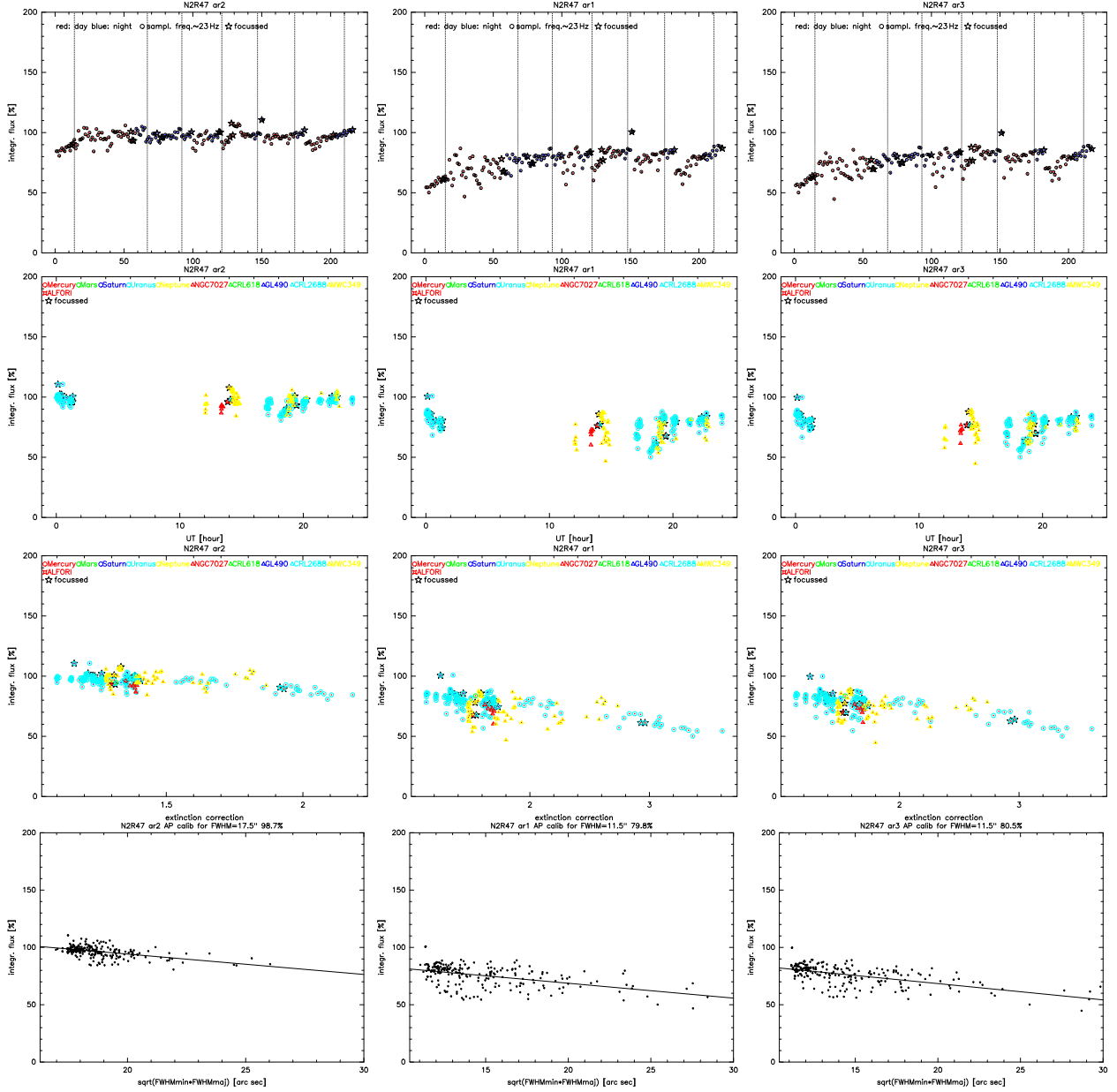


Figure 5: NIKA2 run 47. Aperture flux as a function of: scan running number; UT; extinction correction; size of the source profile. All scans performed on calibrators are shown, including pointing scans and focus sequences. Several effects are visible (see main text). Left, central, right panels belong to Ar2, 1, 3, respectively.

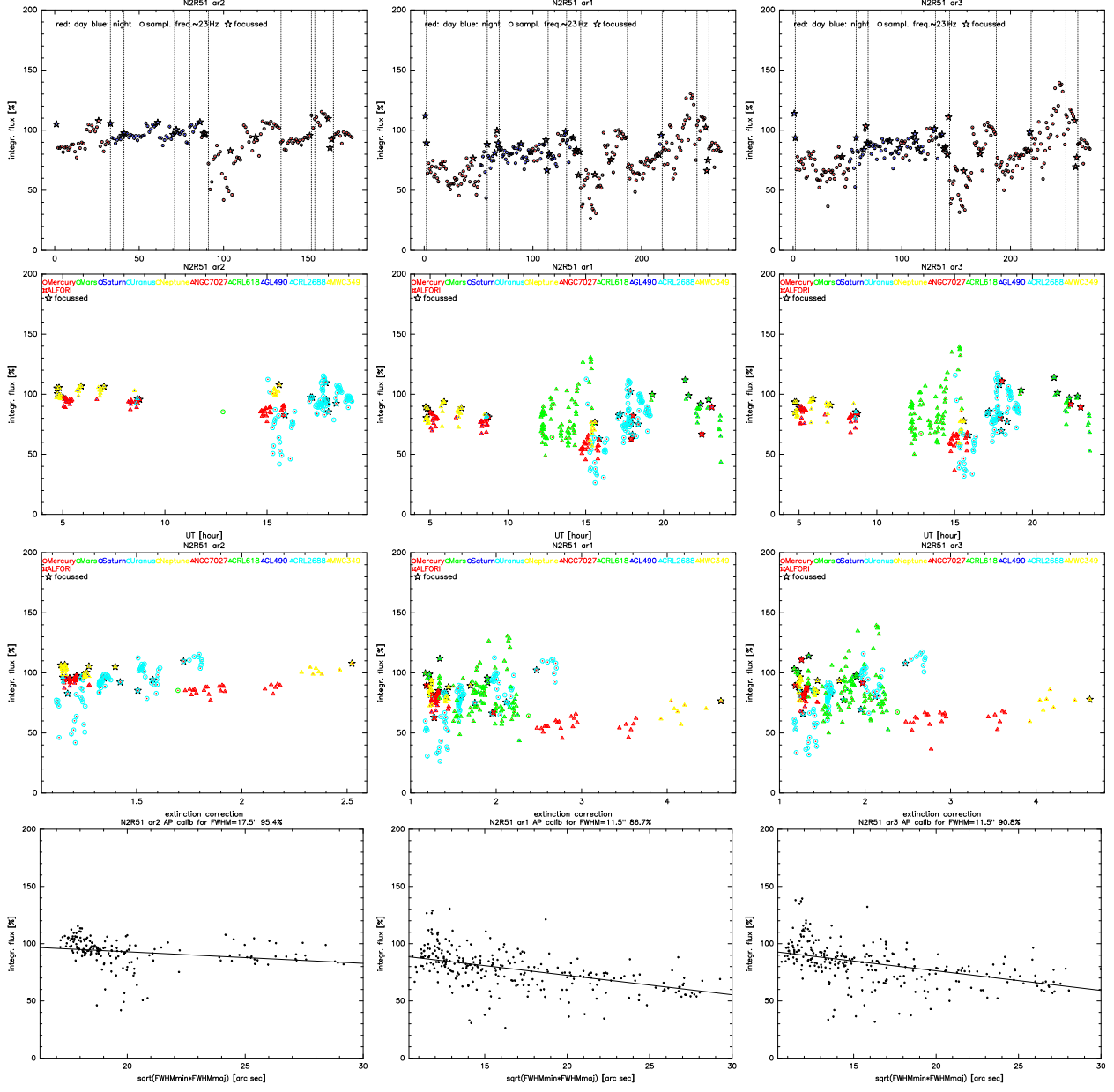


Figure 5: continued: NIKA2 run 51. Note that the points in excess of 100% flux are due to data instabilities. Run 51 shows the highest calibration variation of all NIKA2 runs so far.

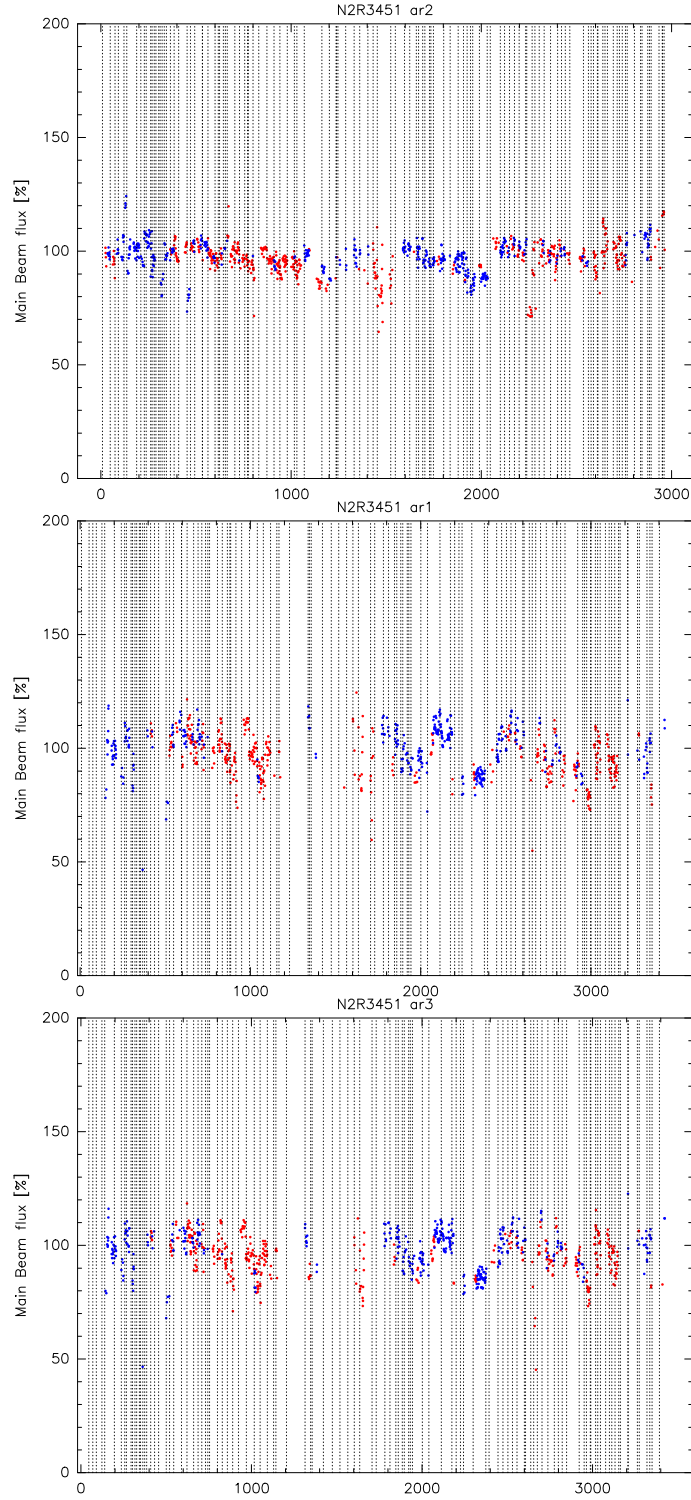


Figure 6: Main beam calibration obtained on all in-focus scans of runs 34 to 51. Vertical lines mark the midnight of different days. The nature of the few-days long drifts is not yet understood.